Finite Element Modeling of the Human Foot and Footwear

Jason Tak-Man Cheung[1,2] and Ming Zhang[1]

[1]Department of Health Technology and Informatics, The Hong Kong Polytechnic University, Hong Kong, China

[2]Human Performance Laboratory, Faculty of Kinesiology, University of Calgary, Calgary, Canada

Abstract: A finite element (FE) model of the human foot and ankle was developed from 3D reconstruction of 2 mm coronal MR images from the right foot of a normal male subject using the segmentation software, Mimics. Solid models of 28 foot bones and encapsulated soft tissue structures models established in Solidworks software were imported into ABAQUS for creating the tetrahedral FE meshes. The plantar fascia and 72 ligaments were defined by connecting the corresponding attachment points on the bones using tension-only truss elements. Contact interactions among the major joints were prescribed to allow relative bone movements. A foot support was used to establish the frictional contact interaction between the foot-support interfaces. The contour of the arch-supporting foot orthoses was obtained from digitization of the subject's foot via a 3D laser scanner. Algorithms were established in Matlab software to create surface models from the digitized foot surface. Solid model of the foot orthoses established in the Solidworks software was properly partitioned in ABAQUS for creating the hexahedral FE meshes. The encapsulated soft tissue and orthotic material were defined as hyperelastic while other tissues were idealized as homogeneous, isotropic and linearly elastic. The ground reaction and extrinsic muscles forces for simulating the stance phase of gait were applied at the inferior ground support and at their corresponding points of insertion by defining contraction forces via axial connector elements, respectively. The FE predictions are being validated by experimental measurements conducted on cadavers and on the same subject who volunteered for the MR scanning.

Keywords: Human Foot and Ankle, Footwear Design, Biomechanics, Hyperfoam, Hyperelasticity, Contact Pressure, Interface Friction, Cadaveric Experiments.

1. Introduction

Many researchers have pointed out that biomechanical factors play an important role on the etiology, treatment and prevention of many foot disorders. Therefore, it is essential to understand the biomechanics associated with the normal foot before any foot orthosis or surgical intervention can be applied. Information on the internal stress and strain of the foot and ankle is essential in

enhancing knowledge on the biomechanical behaviour of the ankle-foot complex. Direct measurement of those parameters is difficult, while a comprehensive computational model can acquire those important clinical information.

The biomechanics of the foot and footwear has been better understood owing to the recent scientific advances in both measurement instrumentation and theoretical methodology. Numerous in vivo experimental studies have been directed to analyze the performance of specific footwear in terms of plantar foot pressure relief or redistribution and its functional role in correcting pathological gait and providing good foot support. Owing to the complexity of the ankle-foot structures and experimental difficulties, most studies focused on the gross joint motions and plantar pressure distribution between the foot and supports. The rationale behind the functional role of footwear on the load distribution and stabilizing ability relies mainly on subjective views, interfacial pressure measurements, or gross motion tracking.

In order to provide a supplement to the experimental inadequacy, many researchers had turned to the computational methods in search of more clinical information. Computational modeling, such as the finite element (FE) method has been used increasingly in many biomechanical investigations with great success due to its capability of modeling structures with irregular geometry and complex material properties, and the ease of simulating complicated boundary and loading conditions in both static and dynamic analyses. The FE method can be an adjunct to experimental approach to predict the load distribution between the foot and different supports, which offer additional information such as the internal stress and strain of the ankle-foot complex. The FE analyses could allow efficient parametric evaluations for the outcomes of the shape modifications and other design parameters of footwear without the prerequisite of fabricated footwear and replicating patient trials.

Existing FE models of the foot or footwear in the literature (Bandak, 2001; Barani, 2005; Camacho, 2002; Chen, 2003; Chu, 1995; Gefen, 2000; Giddings, 2000; Goske, 2005; Jacob, 1999; Lemmon, 1997; Lewis, 2003; Nakamura, 1981; Shiang, 1997; Syngellakis, 2000; Verdejo, 2004) were developed under certain simplifications and assumptions such as a simplified or partial foot shape, assumptions of linear material properties, infinitesimal deformation and linear boundary conditions without considering friction and slip. Although several 3D foot models were developed recently to study the biomechanical behaviour of the human foot and ankle, a geometrically detailed and material realistic 3D FE model of the human foot and ankle specialized for footwear or orthotic design has not been reported.

In this paper, the establishment of a comprehensive FE model of the human foot and ankle was described. The developed FE model was used to quantify the biomechanical interaction among bones, ligaments, interaction between foot plantar and different supports under various loading conditions. The capability of the model to quantify the biomechanical effects of varying geometrical and material factors of different structures of the foot and to predict different surgical outcomes and orthotic performances was discussed.

2. Methods

2.1 Geometrical Properties of the Finite Element Model

The geometry of the human foot and ankle for building the FE model was obtained from 3D reconstruction of coronal magnetic resonance (MR) images from the right foot of a normal male subject of age 26, height 174 cm and weight 70 kg in the neutral foot position. A custom ankle-foot orthosis fabricated during upright sitting of the subject was used to maintain the neutral foot position of the supine lying subject during MR scanning. For the sake of maintaining image quality and avoiding unnecessary details of the surface texture of the foot bones, MR images with 2 mm intervals were chosen.

The MR images were segmented using MIMICS v7.10 (Materialise, Leuven, Belgium) to obtain the boundaries of skeleton and skin surface (Figure 1(a)). For the sake of simplification, the articular cartilages of the bones are fused with their corresponding bone surfaces in the segmentation process. The boundary surfaces of the skeletal and skin components were processed using SolidWorks v2001 (SolidWorks Corporation, Massachusetts, USA) to form solid models for each bone and the whole foot surface. The solid model was then imported and assembled in the FE package ABAQUS v6.4 (Hibbitt, Karlsson and Sorensen, Inc., Pawtucket, RI, USA.).

The FE model of the human foot and ankle, as shown in Figure 1(b), consisted of 28 bony segments, including the distal segments of the tibia and fibula and 26 foot bones: talus, calcaneus, cuboid, navicular, 3 cuneiforms, 5 metatarsals and 14 components of the phalanges embedded in a volume of encapsulated bulk soft tissue. The phalanges were connected together using 2 mm thick solid elements, which simulated the connection of the cartilage and other connective tissues. The interaction among the metatarsals, cuneiforms, cuboid, navicular, talus, calcaneus, tibia and fibula were defined as contacting elastic bodies to allow the simulation of relative bone movement.

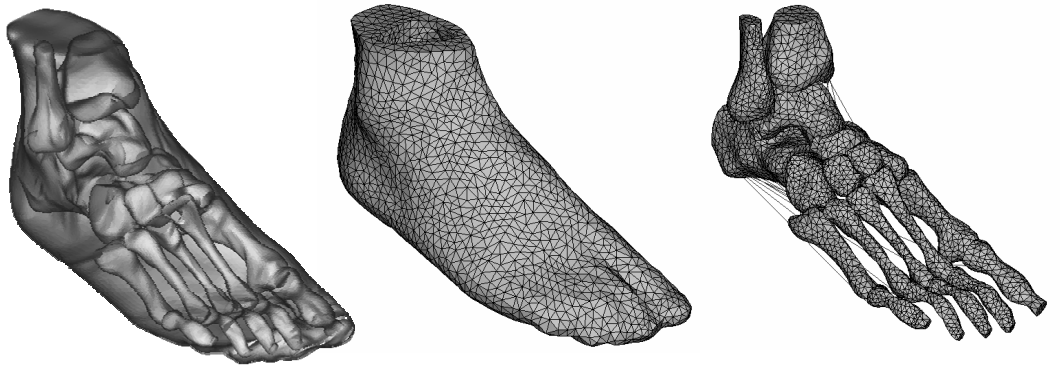

Figure 1. (a) Surface model and (b) FE meshes of the encapsulated soft tissue and bony structures.

Except the collateral ligaments of the phalanges and other connective tissue, a total number of 72 ligaments and the plantar fascia were included and defined by connecting the corresponding attachment points on the bones. Information on the attachment points of the ligamentous structures was obtained from the Interactive foot and ankle (Primal Picture Ltd., London, U.K., 1999). All the bony and ligamentous structures were embedded in a volume of soft tissues.

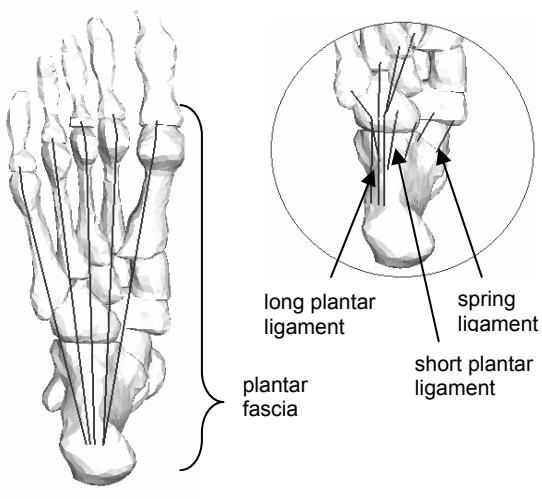

Figure 2. The attachment points of the plantar fascia, spring ligaments, long and short plantar ligaments of the FE model.

The attachment points of the major plantar ligamentous structures such as the plantar fascia, long plantar ligament, short plantar ligament and spring ligament are depicted in Figure 2. The plantar fascia were divided into 5 rays of separate sections, linking the insertions between the calcaneus and the metatarsophalangeal joints.

A variety of solids elements in ABAQUS package can be used to model the foot and ankle structures. Among all the continuum elements, the hexahedra (brick) elements usually provide solution with a higher accuracy at less cost especially with analysis considering geometrically complex structure undergoing large deformations. However, because of the limitation for the automatic-meshing algorithms in ABAQUS to produce hexahedral meshes (brick elements) for those irregularly shaped structures, tetrahedral elements were used for meshing the foot bones and encapsulated soft tissue. The bony and encapsulated soft tissue structures were meshed with 4-noded tetrahedral elements.

For the sake of geometrical simplification, truss elements were used to represent the ligamentous structures of the FE model. As the ligaments were assumed to sustain tensile force only, the no-compression option in ABAQUS was used to modify the elastic behaviour of the material so that compressive stress cannot be generated. In the current FE model, a total number of 98 tension-only truss elements were used to represent the ligaments and the plantar fascia.

To simulate the surface interactions among the bony structures, ABAQUS automated surface-to-surface contact algorithm was used. Because of the lubricating nature of the articulating surfaces, the contact behaviour between the articulating surfaces can be considered frictionless. The overall joint stiffness against shear loading was assumed to be governed by the surrounding ligamentous and encapsulated soft tissue structures together with the contacting stiffness between the adjacent contoured articulating surfaces. Frictionless surface-to-surface contact behaviour was defined between the contacting bony structures. Contact stiffness resembling the softened contact behaviour of the cartilaginous layers (Athanasiou, 1998) was prescribed between each pair of contact surfaces to simulate the covering layers of articular cartilage.

To simulate barefoot stance, a horizontal concrete support was used to establish the foot-ground interface. The horizontal ground support was meshed with hexahedral elements. The same contact modeling algorithm was used to establish the contact simulation of the foot-ground interface with an additional frictional property assigned to model the frictional contact behaviour between the foot-support interface. The coefficient of friction between the foot and ground was taken as 0.6 (Zhang, 1999).

The geometry of the foot orthosis was obtained from the barefoot shape of the same subject who underwent the MR scanning for the development of the aforementioned foot and ankle model. The 3D foot shape of the subject was obtained from surface digitization via a 3D laser scanner (INFOOT Laser Scanner, I-Ware Laboratory Co. Ltd.). Algorithms were established in Matlab v7.0 (Mathworks, Inc) to create surface models for the insole and midsole from the digitized foot surface, which were transferred to SolidWorks v2001 for creation of solid models of variable thicknesses (Figure 3).

The solid model of the foot orthosis was then imported into ABAQUS for the creation of FE mesh. In order to enhance the accuracy of the FE analysis, the foot orthosis was properly partitioned for the creation of a FE mesh of hexahedral elements. The FE mesh of the foot orthosis (Figure 4) composed of an insole layer, a midsole layer and an outsole layer. The same frictional contact modeling approach was used to establish the contact simulation of the foot-insole interface.

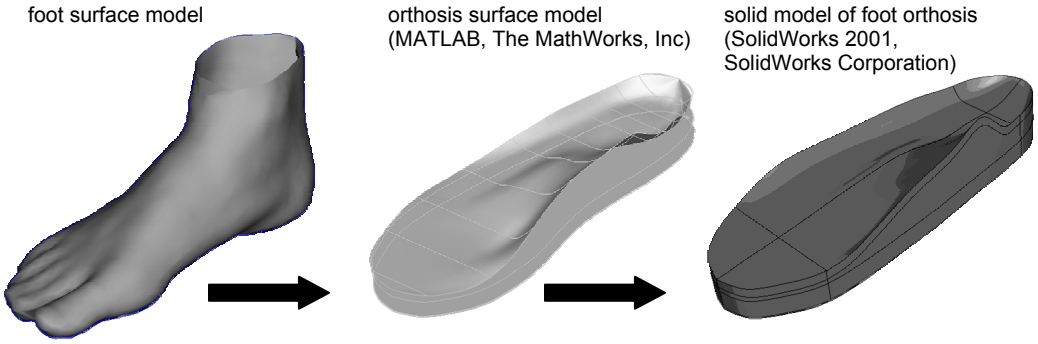

Figure 3. Procedures for creating the foot orthosis model.

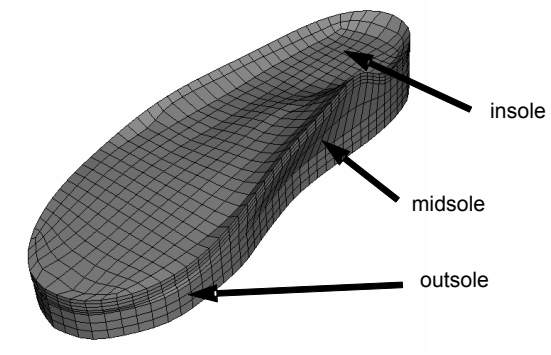

Figure 4. The FE mesh of the foot orthosis.

2.2 Material Properties of the Finite Element Model

Except for the encapsulated soft tissue, all other tissues were idealized as homogeneous, isotropic and linearly elastic (Table 1). The effective Young's modulus and Poisson's ratio for the bony structures were assigned as 7300 MPa and 0.3, respectively, according to the model developed by Nakamura (1981). These values were estimated by averaging the elasticity values of cortical and trabecular bones in terms of their volumetric contribution. The Young's modulus of the cartilage (Athanasiou, 1998), ligaments (Siegler, 1988) and the plantar fascia (Wright, 1964) were selected from the literature. The cartilage was assigned with a Poisson's ratio of 0.4 for its nearly incompressible nature. The ligaments and the plantar fascia were assumed to be incompressible.

Table 1. Material properties and element types defined in the FE model.

Component	Element Type	Young's Modulus E (MPa)	Poisson's Ratio ν	Cross-sectional Area (mm^2)
Bony Structures	3D-Tetrahedra	7,300	0.3	-
Encapsulated Soft Tissue	3D-Tetrahedra	Hyperelastic	-	-
Cartilage	3D-Tetrahedra	1	0.4	-
Ligaments	Tension-only Truss	260	-	18.4
Fascia	Tension-only Truss	350	-	58.6
Foot Orthosis	3D-Brick	Hyperfoam	-	-
Ground Support	3D-Brick	17,000	0.1	-

The encapsulated soft tissue of the FE model was defined as hyperelastic. The hyperelastic material model defined in ABAQUS was employed to represent the incompressible and nonlinearly elastic nature of bulk soft tissue. The stress–strain data on the plantar heel pad (Figure 5) were adopted from the in vivo ultrasonic measurements by Lemmon (1997) to represent the stiffness of the encapsulated soft tissue. A second-order polynomial strain energy potential (ABAQUS, 2004) was adopted with the form

$$U = \sum_{i+j=1}^{2} C_{ij} (\overline{I}_1 - 3)^i (\overline{I}_2 - 3)^j + \sum_{i=1}^{2} \frac{1}{D_i} (J_{el} - 1)^{2i} \tag{1}$$

where U is the strain energy per unit of reference volume; C_{ij} and D_i are material parameters (Table 2); $\overline{I}_1$ and $\overline{I}_2$ are the first and second deviatoric strain invariants defined as

$$\overline{I}_1 = \overline{\lambda}_1^{\,2} + \overline{\lambda}_2^{\,2} + \overline{\lambda}_3^{\,2} \ , \tag{2}$$

$$\overline{I}_2 = \overline{\lambda}_1^{\,(-2)} + \overline{\lambda}_2^{\,(-2)} + \overline{\lambda}_3^{\,(-2)} \ , \tag{3}$$

with the deviatoric stretches

$$\overline{\lambda}_i = J_{el}^{\,-1/3} \lambda_I \ . \tag{4}$$

J_{el} and λ_i are the elastic volume ratio and the principal stretches, respectively.

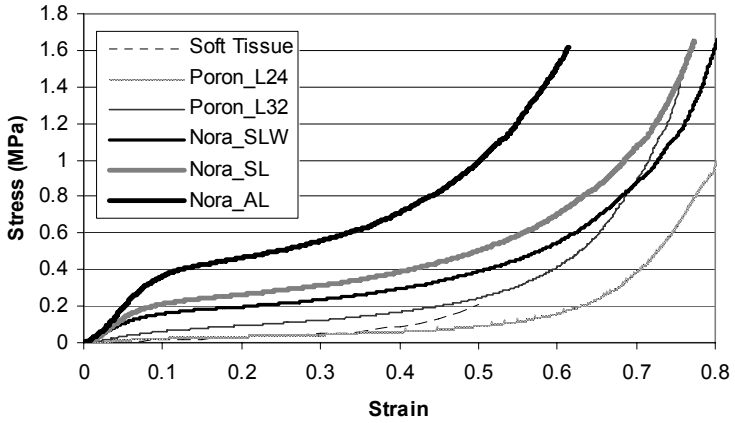

Figure 5. Stress-strain curves for nonlinear material models for encapsulated soft tissue and different orthotic materials.

Table 2. The coefficients of the hyperelastic material model used for the encapsulated soft tissue.

C_{10}	C_{01}	C_{20}	C_{11}	C_{02}	D_1	D_2
0.08556	-0.05841	0.03900	-0.02319	0.00851	3.65273	0.00000

Most elastomers have very little compressibility and their mechanical behaviour can be accurately modeled by the hyperelastic material model. However, rubberlike material for the fabrication of foot orthosis such as elastomeric foam is very compressible and a different strain-energy function is needed to describe the mechanical behaviour of this elastomeric material. Common examples of elastomeric foam materials are cellular polymers such as cushions, padding, and packaging materials.

For the material properties of the foot orthosis in the current FE model, two commonly used elastomeric foam materials for fabricating foot orthosis in our research centre: Poron® (Rogers Corporation, Connecticut, U.S.A) and Nora® (Freudenberg, Germany) were analyzed. Poron® is open-cell polyurethane foams, which are commonly used for cushioning in footwear or insole. Nora® is close-cell Ethylene Vinyle Acetate (EVA) foam, which is available in wide range of densities and stiffness for fabricating insole, midsole or outsole of the shoes. Two different grades of Poron® with Shore A hardness 10^0 (Poron_L24) and 20^0 (Poron_L32) and three different Nora® material of hardness 30^0(Nora_SLW), 40^0(Nora_SL), and 50^0(Nora_AL) were analysed. Hardness of orthotic material was measured using a Shore A type durometer.

The elastic foam energy function (ABAQUS, 2004) employed for describing the highly compressible and nonlinearly elastic behaviour of orthotic material has the form

$$U = \sum_{i=1}^{2} \frac{2\mu_i}{\alpha_i^2}\left[\hat{\lambda}_1^{\alpha_i} + \hat{\lambda}_2^{\alpha_i} + \hat{\lambda}_3^{\alpha_i} - 3 + \frac{1}{\beta_i}(J_{el}^{-\alpha_i\beta_i} - 1)\right] \tag{5}$$

where U is a second order, isotropic hyperfoam strain energy potential per unit of reference volume; $\hat{\lambda}_i$ are principal stretches and J_{el} is the elastic volume ratio. μ_i, α_i and β_i are material parameters.

Each of the orthotic material was tested in a Hounsfield material testing machine (Model H10KM, Hounsfield Test Equipment, UK) with a 1 kN load cell. Samples with 20 mm in diameter and 6 mm in thickness were tested under uniaxial compression of up to 500 N with a testing speed of 1 mm/s. The stress–strain data for different hardness of Poron and Nora material (Figure 5) was used to extract the material parameters of the hyperfoam material model (Table 3) in ABAQUS.

Table 3. The coefficients of the hyperfoam material model used for orthotic materials.

Orthotic Material	μ_1	μ_2	α_1	α_2	β_1	β_2
Poron_L24	0.213	-0.06209	10.3	-3.349	0.32	0.32
Poron_L32	-0.3365	-0.08731	7.272	-2.391	0.32	0.32
Nora_SLW	0.9754	-0.2914	8.87	-2.884	0.32	0.32
Nora_SL	1.037	-0.3044	7.181	-2.348	0.32	0.32
Nora_AL	8.874	-7.827	2.028	1.345	0.32	0.32

2.3 Loading and Boundary Conditions of the Finite Element Model

Double-limb balanced standing and midstance were simulated. In order to simulate the physiological loading on the foot, information on the centre of pressure, total ground reaction forces and foot-shank position, which can be measured from the plantar pressure measuring system and human motion analysis system, should first be known. For a subject with body mass of 70 kg, a vertical force of approximately 350N is applied on each foot during balanced standing. For the simulation of balanced standing, only the Achilles tendon loading was considered while other intrinsic and extrinsic muscle forces were neglected. Force vectors, corresponding to half of the body weight, and the reaction of the Achilles tendon were applied. Five equivalent force vectors representing the Achilles tendon tension were applied at the points of insertion by defining contraction forces via five axial connector elements (Figure 6). The ground reaction force was applied as a concentrated force underneath the ground support. The superior surface of the soft tissue, distal tibia and fibula was fixed throughout the analysis. The ankle joint was assumed to be in its neutral position during balanced standing. The Achilles tendon forces required for simulating the upright balanced standing posture were estimated by matching the FE predictions with the measured plantar pressure distribution and location of centre of pressure of the same subject who volunteered for the MR scanning.

For simulated midstance, the ground reaction and the active extrinsic muscle forces were applied. The geometrical information of the muscular insertion points were obtained from the Interactive Foot and Ankle (Interactive foot and ankle, 1999, Primal Picture Ltd., UK). The extrinsic muscles forces during midstance were estimated from muscles cross-sectional area (Dul, 1983) and electromyography (EMG) data (Perry, 1992) with a linear EMG-force assumption (Kim, 2001). Fine adjustment on the applied muscles forces were made to match the measured centre of pressure of the subject. Musculotendon forces were applied at their corresponding points of insertion by defining contraction forces via axial connector elements (Figure 6). Again, the ground reaction force was applied as a concentrated force underneath the ground support and the superior surface of the soft tissue, distal tibia and fibula was fixed throughout the analysis. The foot-shank position during midstance was measured from the subject.

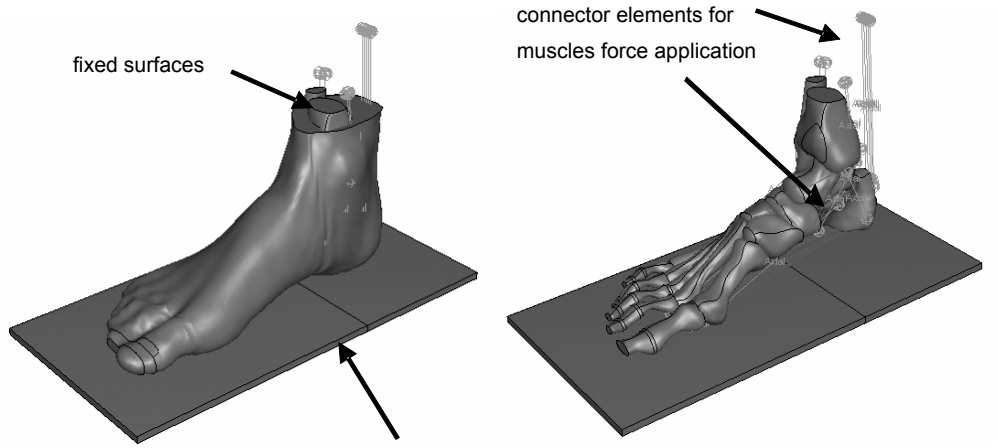

Figure 6. Loading and boundary conditions for simulating the physiological loading on the foot.

2.4 Parametrical Studies

The developed FE model is the first model in the literature to take into account the actual 3D ankle/foot geometry and nonlinearities from material properties, large deformations and interfacial slip/friction conditions (Cheung, 2005b). Throughout the development process of the FE model, parametrical analyze were done to evaluate the sensitivity of different model parameters such as the stiffness of encapsulated bulk soft tissue (Cheung, 2005b) and plantar fascia (Cheung, 2004), Achilles tendon forces (Cheung, 2006a). The ability of the FE model to simulate different surgical and pathological conditions including plantar fasciotomy, (Cheung, 2006b) posterior tibial tendon dysfunction (Cheung, 2006c) and the interactions with different foot supports (Cheung, 2005a, 2006b) was evaluated by comparing the FE predictions to the experimental measurements.

3. Results and Discussion

In this study, a three-dimensional FE model of the human foot and ankle was developed from reconstruction of MR images. The developed FE model, which took into consideration the nonlinearities from material properties, large deformations and interfacial slip/friction conditions

consisted of 28 contacting bony structures, 72 ligaments and the plantar fascia embedded in a volume of encapsulated soft tissue. The FE predictions were found to be reasonably complied with the clinical and experimental observations.

In the parametrical analyses of the FE foot model, the effect of varying stiffness of the encapsulated bulk soft tissue and the plantar fascia was investigated. An increase in bulk soft tissue stiffness from 2 and up to 5 times the normal values was used to approximate the pathologically stiffened tissue behaviour with increasing stages of diabetic neuropathy. The results showed that increasing soft tissue stiffness led to a decrease in the total contact area between the plantar foot and the horizontal support surface and pronounced increases in peak plantar pressure at the forefoot and rearfoot regions. The effect of bulk soft tissue stiffening on bone stress was found to be minimal. A sensitivity study was conducted to evaluate the biomechanical effects of varying elastic modulus (0–700 MPa) of the plantar fascia. The plantar fascia was found to be an important stabilizing structure of the longitudinal arch of human foot during weight-bearing and decreasing the stiffness of plantar fascia would reduce the arch height, increase the strains of the long and short plantar and spring ligaments. In addition, surgical releases of partial and the entire plantar fascia were simulated. Plantar fascia release (PFR) increased the strains of the plantar ligaments and intensified stress in the midfoot and metatarsal bones. Partial and total PFR decreased arch height and resulted in midfoot pronation but did not lead to the total collapse of foot arch even with additional dissection of the long plantar ligaments. The FE model implicated that PFR may provide relief of focal stresses and associated heel pain. However, these surgical procedures may pose a risk of developing arch instability and clinically may produce midfoot pain. The FE predictions suggested that the initial strategy for treating plantar fasciitis should be nonoperative. Surgical release of the plantar fascia, if necessary, should consider only partial release of the plantar fascia to minimize the effect on its structural integrity.

The biomechanical effects of Achilles and posterior tibial tendon loading were investigated. A positive correlation between Achilles tendon loading and plantar fascia tension was found. With the total ground reaction forces of one foot maintained at 350 N to represent half body weight, an increase in Achilles tendon load from (0-700 N) resulted in a general increase in total force and peak plantar pressure at the forefoot. There was a lateral and anterior shift of the centre of pressure and a reduction in the arch height with an increasing Achilles tendon load. From the FE predictions of simulated balanced standing, Achilles tendon forces of 75% of the total weight on the foot (350N) were found to provide the closest match of the measured centre of pressure of the subject during balanced standing. Both the weight on the foot and Achilles tendon loading resulted in an increase in tension of the plantar fascia with the latter showing a two-times larger straining effect. From the FE predictions, overstretching of the Achilles tendon and tight Achilles tendon are plausible mechanical factors for overstraining of the plantar fascia and subsequent development of plantar fasciitis or heel pain. The effect of posterior tibial tendon dysfunction (PTTD) on intact and flat-arched foot structures was investigated during simulated midstance. Unloading the posterior tibial tendon increased the arch deformation and strains of the plantar ligaments especially the spring ligament. The arch-flattening effect of PTTD was smaller than that from PFR. The lack of foot arch support with PFR and PTTD may lead to attenuation of surrounding soft tissue structures and elongation of foot arch, resulting in a progressive acquired flatfoot deformity.

The developed FE model can be used in clinical applications to investigate the foot behaviour of different gait pattern and to design a good foot support. In terms of orthotic/footwear design, the FE model could allow efficient parametric evaluations for the outcomes of the shape modifications and other design parameters of the orthosis without the prerequisite of fabricated orthosis and replicating patient trials. Figure 7 depicts the FE model for simulating the foot-support interface and FE predicted plantar pressure distributions with flat and arch-supporting foot orthoses.

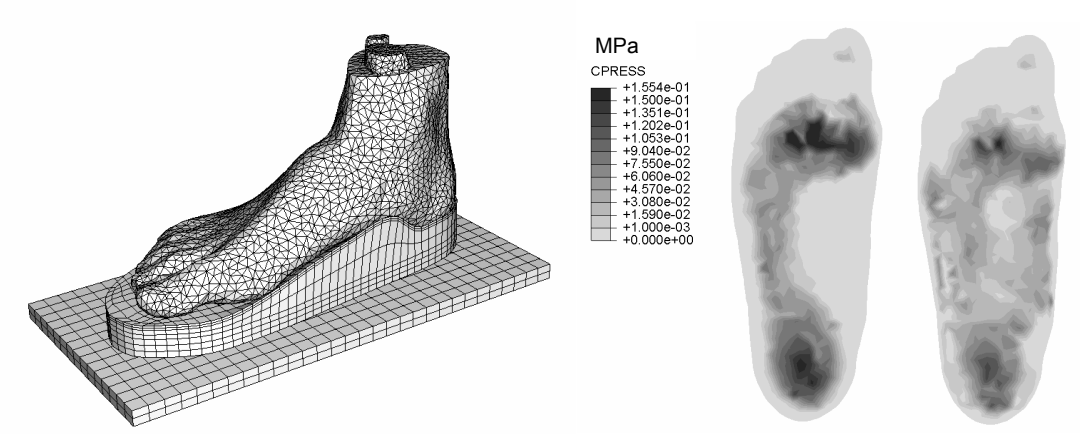

Figure 7. The (a) FE model for simulating the foot-support interace and the (b) FE predicted plantar pressure distributions in contact with flat and arch-supporting foot orthoses.

From the parametrical analyses of the FE model, the custom-molded shape was found to be a more important design factor in reducing peak plantar pressure than the stiffness of the orthotic material. Besides the use of an arch-supporting foot orthosis, the insole stiffness was found to be the second most important factor for peak pressure reduction. Other design factors contributed to a less obvious role in peak pressure reduction in the order of insole thickness, midsole stiffness and midsole thickness. Custom pressure-relieving foot orthosis providing total contact fit of the plantar foot of the diabetic patients during weight-bearing was an important treatment strategy for plantar pressure related diabetic ulceration. A custom orthotic device and extra-depth footwear should be prescribed to diabetic patients at risk of plantar ulceration whenever possible and available.

4. Conclusions

Because of the difficulties to understand the biomechanics of the complicated human foot and ankle structures from experimental studies alone, computational model is needed to provide a viable alternative to predict their biomechanical behaviour. In this study, a 3D FE model of the

human foot and ankle was developed from 3D reconstruction of MR images from the right foot of a male adult subject. The developed FE model, which took into consideration the nonlinearities from material properties, large deformations and interfacial slip/friction conditions consisted of 28 contacting bony structures, 72 ligaments and the plantar fascia embedded in a volume of encapsulated soft tissue. The developed geometrically accurate 3D FE models of the foot and ankle considered the first time in the literature the relative motion of all the major foot joints by a surface-to-surface contact approach as well as realistic nonlinear material properties of the encapsulated soft tissue.

With further improvement and development of the FE model, the FE predictions on the biomechanical effect of different types of foot orthosis can be used to refine the design principles of orthosis in the CAD/CAM process in terms of appropriate shape and material of the orthosis in order to fit specific functional requirements of the subject and individual foot structure. Comprehensive knowledge-based criteria for footwear design can be established to provide systemic guidelines for clinicians to prescribe and fabricate an optimized footwear to maximize its functions as well as the subjects' comfort and gait performance.

5. References

ABAQUS theory and user's manual, version 6.4, 2004. Hibbitt, Karlsson and Sorensen Inc., Pawtucket, RI, USA.

Athanasiou, K.A., Liu, G.T., Lavery, L.A., Lanctot, D.R., Schenck, R.C., "Biomechanical topography of human articular cartilage in the first metatarsophalangeal joint," Clinical orthopaedics, vol. 348, pp. 269-281, 1998.

Bandak, F.A., Tannous, R.E., Toridis, T., "On the development of an osseo-ligamentous finite element model of the human ankle joint," International Journal of Solids and Structures, vol. 38, pp. 1681-1697, 2001.

Barani, Z., Haghpanahi, M., Katoozian, H., "Three dimensional stress analysis of diabetic insole: a finite element approach," Technology and Health Care, vol. 13, pp. 185-192, 2005.

Camacho, D.L.A., Ledoux, W.R., Rohr, E.S., Sangeorzan, B.J., Ching, R.P., "A three-dimensional, anatomically detailed foot model: A foundation for a finite element simulation and means of quantifying foot-bone position," Journal of Rehabilitation Research and Development, vol. 39, pp. 401-410, 2002.

Chen, W.P., Ju, C.W., Tang, F.T., "Effects of total contact insoles on the plantar stress redistribution: a finite element analysis," Clinical Biomechanics, Vol. 18, pp. S17-24, 2003.

Cheung, J.T., Zhang, M., An, K.N., "Effects of plantar fascia stiffness on the biomechanical responses of the ankle-foot complex," Clinical Biomechanics, vol. 19, pp. 839-846, 2004.

Cheung, J.T., Zhang, M., "A 3D finite element model of the human foot and ankle for insole design," Archives of Physical Medicine and Rehabilitation, vol. 86, pp. 353-358, 2005a.

Cheung, J.T., Zhang, M., Leung, A.K., Fan, Y.B., "Three-dimensional finite element analysis of the foot during standing - A material sensitivity study," Journal of Biomechanics, vol. 38, pp. 1045-1054, 2005b.

Cheung, J.T., Zhang, M., An, K.N., "Effect of Achilles tendon loading on plantar fascia tension in the standing foot," Clinical Biomechanics, Vol. 21, pp. 194-203, 2006a.

Cheung, J.T., An, K.N., Zhang, M., "Consequences of Partial and Total Plantar Fascia Release: A Finite Element Study," Foot and Ankle International, Vol 27, pp. 125-132, 2006b.

Cheung, J.T.M., "Development of knowledge-based criteria for designing foot orthoses," Ph.D. Thesis, The Hong Kong Polytechnic University, 2006c.

Chu, T.M., Reddy, N.P., Padovan, J., "Three-dimensional finite element stress analysis of the polypropylene, ankle-foot orthosis: static analysis," Medical Engineering and Physics, vol. 17, pp. 372-379, 1995.

Dul, J., "Development of a minimum-fatigue optimization technique for predicting individual muscle forces during human posture and movement with application to the ankle musculature during standing and walking," Ph.D. Thesis, Vanderbilt University, 1983.

Gefen, A., Megido-Ravid, M., Itzchak, Y., Arcan, M., "Biomechanical analysis of the three-dimensional foot structure during gait: a basic tool for clinical applications," Journal of biomechanical engineering, vol. 122, pp. 630–639, 2000.

Giddings, V.L., Beaupre, G.S., Whalen, R.T., Carter, D.R., "Calcaneal loading during walking and running," Medicine and science in sports and exercise, vol. 32, pp. 627-634, 2000.

Goske, S., Erdemir, A., Petre, M., Budhabhatti, S., Cavanagh, P.R., "Reduction of plantar heel pressures: Insole design using finite element analysis," Journal of Biomechanics, in press, 2005.

Jacob, S., Patil, M.K., "Stress analysis in three-dimensional foot models of normal and diabetic neuropathy," Frontiers of Medical and Biological Engineering, vol. 9, pp. 211-227, 1999.

Kim, K.J., Kitaoka, H.B., Luo, Z.P., Ozeki, S., Berglund, L.J., Kaufman, K.R., An, K.N., "An in vitro simulation of the stance phase in human gait," Journal of Musculoskeletal Research, vol. 5, pp. 113-121, 2001.

Lemmon, D., Shiang, T.Y., Hashmi, A., Ulbrecht, J.S., Cavanagh, P.R., "The effect of insoles in therapeutic footwear: a finite-element approach," Journal of Biomechanics, vol. 30, pp. 615-620, 1997.

Lewis, G., "Finite element analysis of a model of a therapeutic shoe: effect of material selection for the outsole," Bio-medical Materials and Engineering, vol. 13, pp. 75-81, 2003.

Nakamura, S., Crowninshield, R.D., Cooper, R.R., "An analysis of soft tissue loadingin the foot-a preliminary report," Bulletin of prosthetics research, vol. 18, pp. 27–34, 1981.

Perry, J., "Gait analysis: normal and pathological function," Publisher Thorofare, N.J.: SLACK. 1992.

Shiang, T.Y., “The nonlinear finite element analysis and plantar pressure measurement for various shoe soles in heel region,” Proceedings of the National Science Council, Republic of China. Part B, Life Sciences, vol. 21, pp. 168-174, 1997.

Siegler, S., Block, J., Schneck, C.D., “The mechanical characteristics of the collateral ligaments of the human ankle joint,” Foot and Ankle, vol. 8, pp. 234-242, 1988.

Syngellakis, S., Arnold, M.A. and Rassoulian, H., “Assessment of the non-linear behaviour of plastic ankle foot orthoses by the finite element method,” Proceedings of the Institution of Mechanical Engineers. Part H, Journal of Engineering in Medicine, vol. 214, pp. 527-539, 2000.

Verdejo, R., Mills, N.J., “Heel-shoe interactions and the durability of EVA foam running-shoe midsoles,” Journal of Biomechanics, vol. 37, pp. 1379-1386, 2004.

Wright, D., Rennels, D., “A study of the elastic properties of plantar fascia,” The Journal of bone and joint surgery. American volume vol. 46, pp. 482-492, 1964.

Zhang, M., Mak, A.F., “In vivo skin frictional properties,” Prosthetics and orthotics international, vol. 23, pp. 135-141. 1999.

6. Acknowledgment

The authors would like to thank Dr. Hector Ma and his departmental staff of the Scanning Department of St. Teresa’s Hospital, Hong Kong for facilitating the MR scanning. The financial support from the Hong Kong Jockey Club endowment, the research grant (A/C No. A-PC91) and research studentship from The Hong Kong Polytechnic University, and the grant from Research Grant Council of Hong Kong (Project No. PolyU 5249/04E, PolyU 5317/05E) are acknowledged.